AlGaN/GaN Based Ultra-wideband 15-W High-Power Amplifier with Improved Return Loss

Jin-Cheol Jeong, Dong-Pil Jang, Dong-Hwan Shin, In-Bok Yom, Jae-Duk Kim, Wang-Youg Lee, and Chang-Hoon Lee

An ultra-wideband microwave monolithic integrated circuit high-power amplifier with excellent input and output return losses for phased array jammer applications was designed and fabricated using commercial 0.25-µm AlGaN/GaN technology. To improve the wideband performance, resistive matching and a shunt feedback circuit are employed. The input and output return losses were improved through a balanced design using Lange-couplers. This three-stage amplifier can achieve an average saturated output power of 15 W, and power added efficiency of 10% to 28%, in a continuous wave operation over a frequency range of 6 GHz to 18 GHz. The input and output return losses were demonstrated to be lower than –15 dB over a wide frequency range.

Keywords: Gallium nitride (GaN), microwave monolithic integrated circuit (MMIC), high power amplifier (HPA), wideband, return loss, electronic warfare (EW).

Manuscript received Dec. 11, 2015; revised Mar. 15, 2016; accepted Apr. 5, 2016.

This work was supported by the Agent for Defense Development, Korea (15AR2200, The wide-band semiconductor phased array transmitter technology).

Jin-Cheol Jeong (corresponding author, jcjung@etri.re.kr), Dong-Pil Jang (dpjang@etri.re.kr), Dong-Hwan Shin (dh-shin@etri.re.kr), and In-Bok Yom (ibyom@etri.re.kr) are with the Broadcasting Media Research Laboratory, ETRI, Daejeon, Rep. of Korea.

Jae-Duk Kim (jaeduk.kim@lignex1.com) and Wang-Yong Lee (wangyong.lee@lignex1.com) are with the EW R&D Lab, LIGNEX1, Yongin, Rep. of Korea.

Chang-Hoon Lee (leech@add.re.kr) is with the 2nd R&D Institute, Agency for Defense Development, Daejeon, Rep. of Korea.

I. Introduction

In electronic warfare jammer systems, solid-state technologies are becoming the best candidates for replacing the traveling wave tube amplifier (TWTA), despite the wider utilization of TWTAs for conventional jammers. Commercially available solid-state power devices have many performance advantages over TWTAs, including a higher reliability, superior intermodulation performance, lower costs for maintenance and spare parts, higher personnel safety, lower power consumption, and soft failure modes [1]. For this reason, to realize phased array antennas for the latest jammer systems, specifically for use within the 6 GHz to 18 GHz band, there has been a strong demand for solid-state monolithic microwave integrated circuit (MMIC) high-power amplifiers (HPAs) with high output power, high efficiency, and wide bandwidth.

Implementations based on aluminum gallium nitride/gallium nitride (AlGaN/GaN) technology for ultra-wideband HPA applications can provide high power, high efficiency, better thermal properties, and a lower dc current compared to MMICs based on gallium arsenide (GaAs) technology owing to their high breakdown voltage and high thermal conductivity [2]. HPAs using a GaN high-electron-mobility transistor (HEMT) with an output power of more than 100 W have been reported for use within high frequency bands (C-, X-, and Ku-bands) [3] through hybrid-type realizations.

Wideband HPAs have been reported mainly through two circuit configurations of a distributed power amplifier (DPA) and a multi-stage reactively matched amplifier, as shown in Table 1. DPAs have typically shown high power and excellent wideband capabilities; however, they suffer from limited gain. TriQuint reported an attractive performance, with a maximum

http://dx.doi.org/10.4218/etrij.16.2615.0020

Table 1. Comparison of wideband power amplifier MMICs measured under CW conditions.

Reference	Technology	Freq. (GHz)	Pout (dBm)	PAE (%)	Gain (dB)	RLmax (dB)	*VD* (V)	Type
This work	0.25 GaN HEMT	6–18	40.4–43.2	10–23	20–29	–15	30	Reactive, Lange coupler
[4]	0.25 GaN HEMT	2–18	40.2–42.2	25–38	9–13	–10	35	Distributed
[5]	0.25 GaN HEMT	6–18	39.0–41.0	19–22	18–22	–7	28	Distributed
[6]	0.25 GaN HEMT	6–18	40.0–41.0	13–20	8–10	–15	40	Distributed, Lange coupler
[7]	0.25 GaN HEMT	6–18	37.5–40.0	13–26	18–24	–3	25	Reactive
[8]	0.25 GaN HEMT	6–18	39.5–41.0	10–24.5	19–28	–10	28	Reactive

output power of 40.2 dBm to 42.2 dBm and an excellent PAE of higher than 25%; however, the reported gain is only around 10 dB [4]. Hittite also provides an HPA product with a 10-W output power and 20-dB gain, but has a poor return loss at high frequency [5]. Considering the module integration, interface capabilities, such as the return loss, are important for reducing unwanted signal loss enhanced by a mismatch between adjacent components. To improve the interface performance, Fujitsu reported a balanced-type HPA using a Lange coupler with a good return loss of lower than –15 dB, but a gain level of lower than 10 dB [6]. Although multi-stage reactively matched amplifier MMICs with parallel matching networks have been reported, they have weak return loss capabilities. UMS demonstrated a reactive-type HPA with a high gain of around 20 dB, but with degraded return losses [7], [8].

In this paper, based on commercial 0.25-µm AlGaN/GaN technology, the development of an ultra-wide MMIC high-power amplifier with an average output power of 15 W over a frequency range of 6 GHz to 18 GHz is described. To the best of the authors' knowledge, this output power measured under continuous wave (CW) conditions is the highest among the reported HPAs. The return loss was improved using input and output Lange couplers, and was lower than –15 dB over a wideband frequency. Based on CW measurements, two types of test fixtures with different materials and shapes were compared in terms of their thermal properties.

II. High-Power Amplifier Design

A three-stage cascaded, reactively matched MMIC HPA was designed using commercial foundry based on a UMS 0.25-µm AlGaN-GaN HEMT with a 100-µm thick SiC substrate [9].

A simplified block diagram of a wideband HPA is shown in Fig. 1. A balanced configuration was employed to improve the

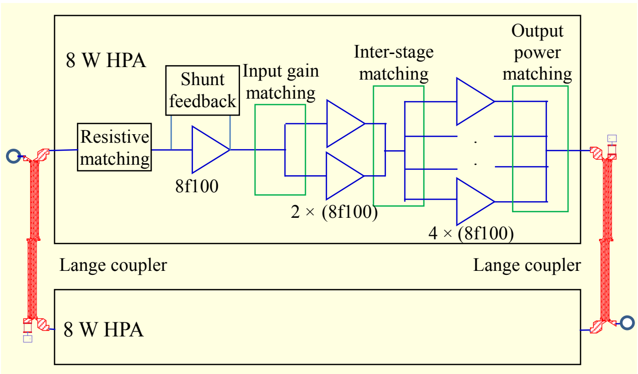

Fig. 1. Simplified block diagram of a reactively matched three-stage wideband 15-W HPA with a balanced configuration.

interface capabilities such as the input and output return losses. A 15-W HPA was realized using two 8-W HPAs combined in-parallel with two Lange couplers, which provides improved input and output return losses. The 8-W HPA employs 1:2:4 gate periphery ratios to provide sufficient power margins between stages. The peripheries of the pHEMTs are 0.8 mm (1 × 8f100 (eight gate fingers and 100-µm unit gate width)), 1.6 mm (2 × 8f100), and 3.2 mm (4 × 8f100) for the first, second, and power stages, respectively. A load-pull simulation was conducted for several sized HEMTs to select the best device periphery for application. An 8f100 HEMT was chosen as the best component in terms of output power, PAE, and gain. Resistive matching and a shunt feedback were used only in the first stage because the circuits have a drawback in terms of lower gain and power capabilities, but have an advantage in terms of their wideband performance. The input-matching and two inter-stage matching networks were optimized for high gain within a wide frequency range, whereas the output matching network was optimized to obtain a higher output power based on the load/source-pull simulations.

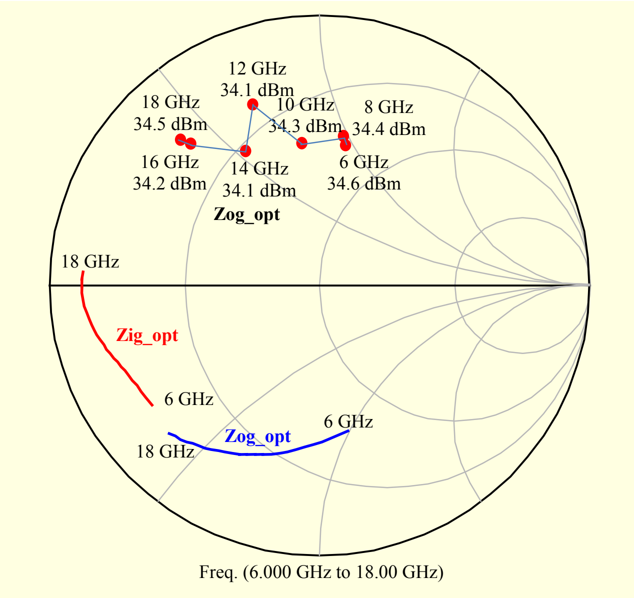

Fig. 2. Optimum impedances of 8f100 HEMT for gain matching and delivered power matching obtained through small signal and load-pull simulations. Values at the optimum power impedances indicate the maximum power levels delivered to the load.

To improve the power efficiency, we adopted a class-AB quiescent bias point. For the selected HEMT with a quiescent bias point of $VD = 30$ V and $VG = -2.6$ V, small signal and load-pull simulations were carried out to obtain the optimum impedance levels for maximum gain and maximum delivered output power, respectively, over a frequency range of 6 GHz to 18 GHz. Figure 2 shows the reflection coefficient calculated using the optimum impedances, which are observed to spread widely on a Smith-chart. The impedances obtained are the input and output impedances of the transistor for maximum gain (Zig_opt and Zog_opt, respectively), and the output impedance for the maximum delivered power (Zop_opt). The maximum delivered output powers for the 8f100 HEMT ranged from 34.1 dBm to 34.6 dBm with a typical 49% PAE under a drain voltage of 30 V and a gate voltage of –2.6 V at 6 GHz to 18 GHz, as shown in Fig. 2. Eight parallel combined 8f100 HEMTs are required to achieve more than 10-W output power considering signal losses induced through wideband matching circuits.

To realize a reactively matched HPA within a wide frequency band, widespread optimum impedances have to be matched to 50 Ω. The first design approach is reducing the spreading range of the impedances, or moving the impedances to the center of the Smith-chart. Resistive matching and a shunt-feedback were adapted for this approach, the circuit of which is shown in Fig. 3. In the resistive matching circuit, a series-connected resistor to the gate of the transistor moves the

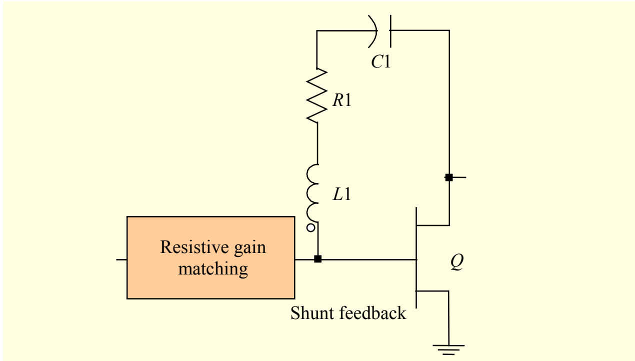

Fig. 3. Schematic circuit diagram of resistive matching and a shunt feedback to achieve wideband matching in a multi-stage reactive-matched HPA (this circuit is employed in the first stage of the 15-W wideband HPA).

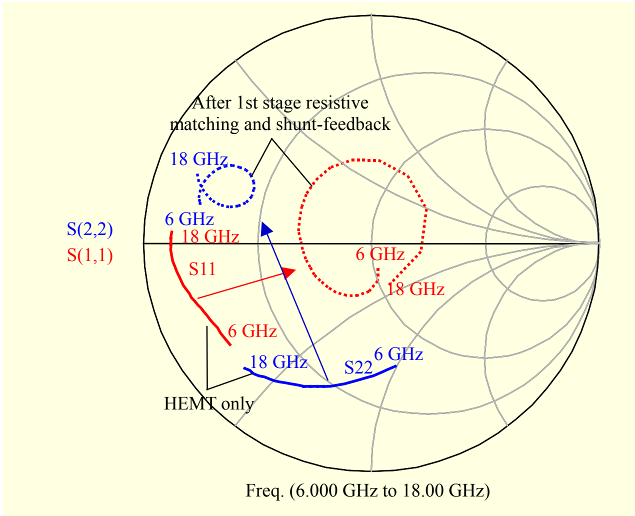

Fig. 4. Input and output impedances of the 8f100 HEMT, and the Impedances after the first-stage design with resistive matching and shunt feedback.

low input impedance to a higher impedance of close to 50 Ω, and improves the input voltage standing wave ratio (VSWR), as shown in Fig. 4. A shunt feedback was realized by serially adding an inductor, a resistor, and a capacitor between the drain and gate ports. The inductor value is selected to be a dominant component for the feedback circuit. The gain at a lower frequency of an HEMT is normally higher than at a higher frequency. The gain at a lower frequency will decrease by the inductor in the feedback circuit, and enhance a flat gain over the wideband frequency. This changes the impedance shape into a circle and reduces the range of spreading.

Figure 4 shows the simulation results for the designed first-stage circuit with resistive matching and shunt feedback of a wideband HPA. The input impedance increases to close to the center of the Smith-chart owing to the input resistor, whereas the shape of the output impedance narrows mainly from the

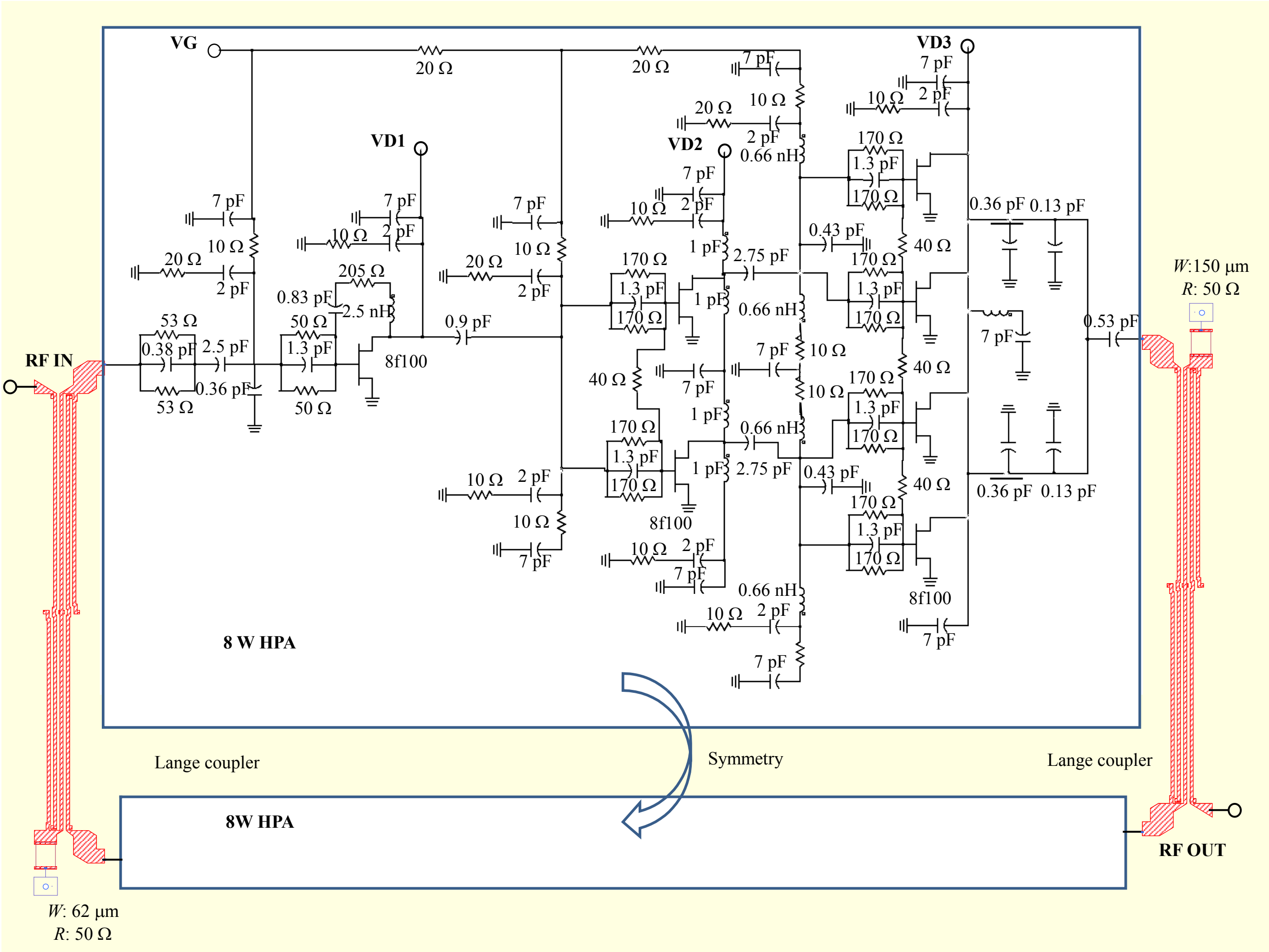

Fig. 5. Detailed schematic circuit diagram of the reactively matched three-stage wideband 15-W HPA with a balanced configuration. Detailed upper circuit block is symmetrically copied to the lower block.

shunt feedback. Impedances at a frequency of lower than 12 GHz decrease more rapidly, resulting in the shrinkage of the output impedance. The shunt feedback affects the input and output impedances. The input impedance at a lower frequency moves more than that at a higher frequency, changing the impedance shape from a straight line to a circle, as shown in Fig. 4.

Figure 5 shows a detailed schematic diagram using the component values. To achieve a stability factor of $K > 1$ over a wide frequency band, a parallel-combined resistor and a capacitor are connected to an input of 8f100 HEMT. The values of the resistor (25 Ω) and capacitor (1.3 pF) were carefully selected to provide no degradation with the maximum output power, sacrificing some gain decrease over a wide frequency band. A resistive matching circuit was implemented using the two parallel-connected resistors (53 Ω) and a capacitor (0.38 pF). The capacitor is required to reduce the losses at a higher frequency. The component values were tuned for a tradeoff between a relative good input VSWR and minimizing loss. A shunt feedback in the first stage is realized using a series-connected 2.5-nH inductor, a 205-Ω resistor, and a 0.83-pF capacitor between the drain port and gate port of the HEMT. The values are tuned for the minimum overall gain slope of the HPA.

Each stage matching was conducted according to the design procedures of a previously reported C-band 50-W HPA [10]. After the port impedance of each matching circuit was set to the optimum impedances at the center frequency of 12 GHz, as shown in Fig. 2, each circuit was designed to provide good input and output return losses over the required wide-frequency band. We adopted a proper matching topology using shunt capacitors instead of open-stubs to achieve a compact design. A short-stub was used in the output matching to improve the wideband power performance, which is shown in the output matching circuit in Fig. 5. It is denoted as an inductor connected to a 7-pF capacitor. In the design of the output stage matching circuit, the eight input port impedances are set to a conjugate value of the optimum power impedance (12.5 + j34) obtained through a load-pull simulation, as shown in Fig. 2. The output matching circuit with eight input ports with a value of (12.5 – j34) and a 50-Ω output port was constructed using micro-strip lines and shunt capacitors. The circuit configuration and component values were optimized to provide good input and output return losses for the matching circuit. After each matching circuit, including the input gain matching circuit, two inter-stage matching circuits, and the output power matching circuit, are designed, they are integrated with HEMTs and used to construct an HPA circuit, as shown in Fig. 5. The values of all components were carefully optimized for the gain, output power, and power efficiency over a wide-frequency band.

Bias lines are realized with micro-strip lines and small-sized inductors for providing short-stubs to contribute to impedance matching instead of an RF chock. All distributed micro-strip lines were fully optimized through an electromagnetic simulation. To improve the power balancing and avoid an odd mode oscillation, 40-Ω resistors are connected between gates of an adjacent parallel HEMT. In the gate and drain bias circuits, a large 7-pF capacitor and small 2-pF capacitors with a series-connected resistor were used for the de-coupling of the low- and high-frequency signals, respectively. The gate pads are connected to each other, and each 8-W HPA block shares the same gate bias pads, whereas the drain biasing must be supplied to each stage and both sides of the 8-W HPA to stay below the rated current limits of the bias lines and preserve the signal balance between parallel combined HEMTs.

Figure 6 shows the small signal performance of the designed single-ended 8-W HPA. The DC voltages, VDS and VGS, were set to +30 V and –2.6 V, respectively, and a 1-A quiescent DC current was supplied. The small signal gain was higher than 21 dB, whereas the input and output return losses were lower than –7 dB over the frequency range of 6 GHz to 18 GHz. The gain at a frequency edge of around 6 GHz and 18 GHz was designed to be higher than at the middle frequency so as to broaden the operating frequency band. This is achieved using an optimization function, the goal of which is to have a higher weight at the edge frequency than at the center frequency. The power performance of the designed 8-W HPA provides 14-W to 17-W of output power with 15% to 25% PAE over the frequency range.

A balanced configuration with Lange couplers provides HPA-protection from reflected power and acts as an isolator in system applications in addition to the advantage of improved return losses. A Lange coupler is a four-port coupled-line hybrid with one port terminated with a 50-Ω resistor. Ideally, it has a 0.5-dB coupling bandwidth of approximately 50% [11]; however, a back-to-back structure serially connected with input and output couplers has a better bandwidth capability. Figure 7 shows a schematic diagram of the back-to-back structure of the input and output Lange couplers used in the wideband 15-W HPA design. The Lange coupler in this design has four fingers, and the length of each finger is 2,200 mm, which provides a center frequency of about 12 GHz. For a tighter coupling, a small spacing is better, and in this design, the finger width and finger spacing were set to 10.0 μm, which is the lower limitation of this process. A 50-Ω load resistor used in the

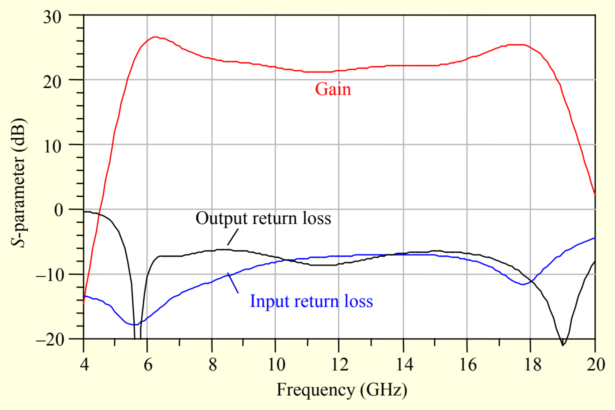

Fig. 6. Small-signal gain, input return loss, and output return loss vs. Frequency of the single-ended 8-W HPA.

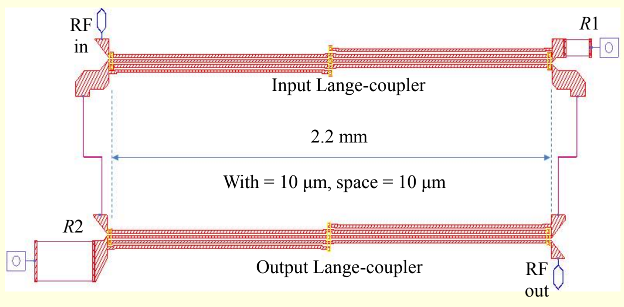

Fig. 7. Two Lange couplers connected back-to-back used in the input and output ports to combine the two single-ended 8-W HPAs.

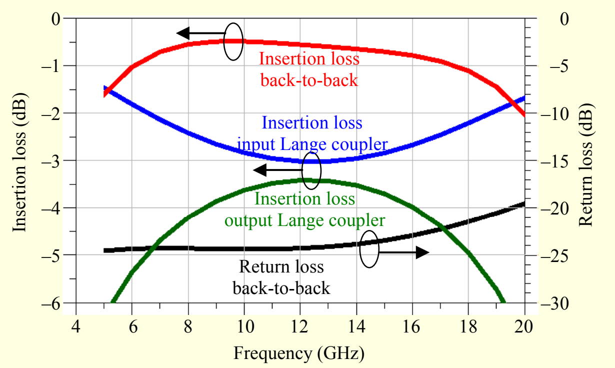

Fig. 8. Insertion and return losses of the designed input/output Lange couplers and their back-to-back circuit.

output Lange coupler has a wide width of 150 μm because it has to sustain high reflected power from the HPA output port, whereas the input coupler has a smaller width of 62 μm.

The simulation results of the back-to-back structure and two single Lange-couplers are shown in Fig. 8. For the center frequency of 12 GHz, the 0.5-dB coupling bandwidth of the back-to-back structure covers from 6 GHz to 18 GHz with a fully low return loss of less than –20 dB, whereas two single couplers have a bandwidth of approximately 7 GHz. The insertion loss of the back-to-back coupler is lower than –1 dB, and typically over –0.7 dB from 6 GHz to 18 GHz. The degradation in output power is estimated to be around –0.35 dB, which can be endured when considering a good port interface.

III. Measured Results and Comparison

Figure 9 shows a microphotograph of the fabricated wideband 15-W MMIC HPA. The size of the chip is 5.5 mm × 5.0 mm with a thickness of 0.1 mm.

The small signal gain and the input and output return losses versus frequency were measured using the probe station measurement system. The gate voltage synchronized to the input signal was pulsed at –2.6 V with a fixed drain bias of 30 V under the conditions of a pulse width of 100 μs and a duty cycle of 10%; in addition, a pulsed 1.9-A DC current is supplied. A comparison of the measured small signal and design results is shown in Fig. 10. The gain with a minimum level of 20 dB is higher than the design at the two frequency edges, which is believed to be due to the minor deviation compared with the model value of some small-sized capacitors of lower than 0.5 pF in the matching circuits. However, the measured data show a similar trend as the design results. The measured input and output return losses are all lower than –15 dB over a wideband frequency, and show good agreement with the design results.

Pulse-mode power measurements were conducted under the same bias and pulse conditions as the small signal measurement using the probe station measurement system. The output power and PAE over a frequency range of 6 GHz to 18 GHz are compared with the design results in Fig. 11. The output power ranges from 40.8 dBm (12.5 W) to 43.8 dBm (24 W) in a wideband frequency, and the average power is around 16 W. The measurement and design show good agreement with a difference of less than 1 dB. The power-added efficiency varies between 12% and 28% with a similar trend as the measured output power, with an average PAE of around 16%.

The measured output power, gain, and PAE as a function of the input power at frequency points of 6 GHz, 12 GHz, and 18 GHz are shown in Fig. 12. The bias and pulse conditions are the same as the above output power measurements. It can be seen that the output power is saturated at an input power of 28 dBm, and the power gain is around 15 dB at the corresponding input power. It was observed that the output power at 12 GHz increases slightly until an input power of 33 dBm and a power gain of 10 dB are achieved, while maintaining the PAE.

A CW measurement was conducted with the MMIC HPA mounted in a test fixture. Differing from the HPAs with a narrow operating frequency band and high PAE, the CW measurement for a wideband HPA with a relatively low PAE was significantly affected by the material properties and shape

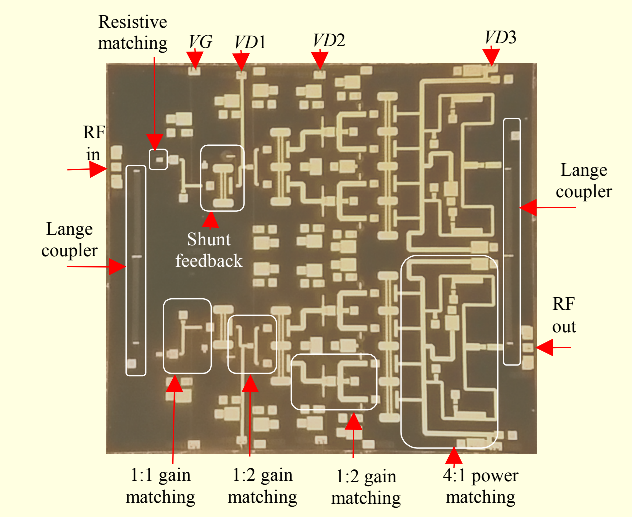

Fig. 9. Microphotograph of the fabricated wideband 15-W MMIC HPA. Chip size is 5.5 mm × 5.0 mm.

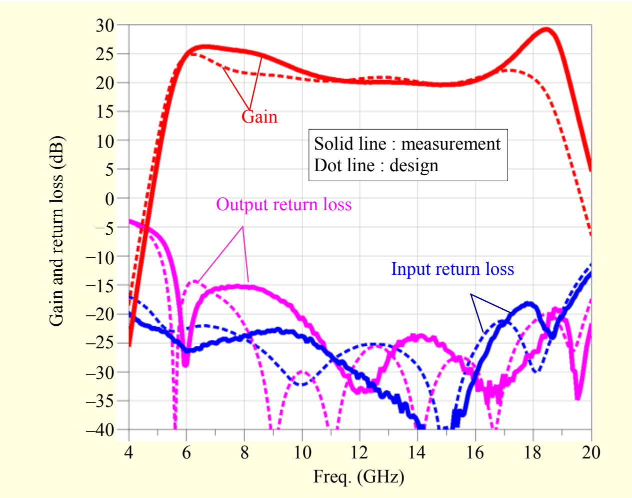

Fig. 10. Measured small signal gain, input return loss, and output return loss vs. frequency of the wideband HPA during pulse mode operation (under the condition of a pulse width of 100 μs and a duty cycle of 10%, and biased at VD = 30 V). Solid and dotted lines indicate the measurement and design results, respectively.

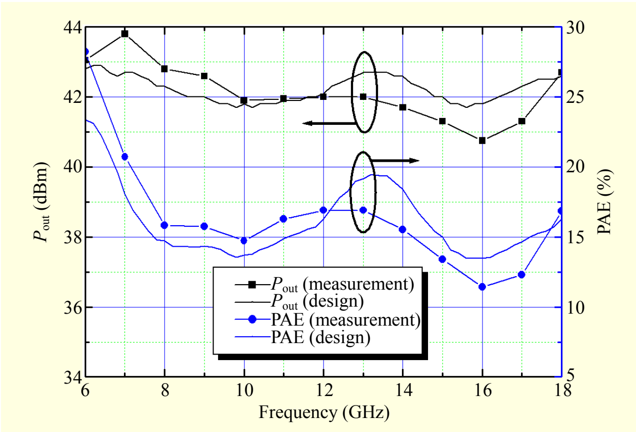

Fig. 11. Measured output power and PAE of the wideband HPA vs. frequency compared to the design performance under a pulse width of 100 µs and a duty cycle of 10%, biased at *VD* = 30 V with 28-dBm input power. Solid and marked solid lines indicate the design and measured results, respectively.

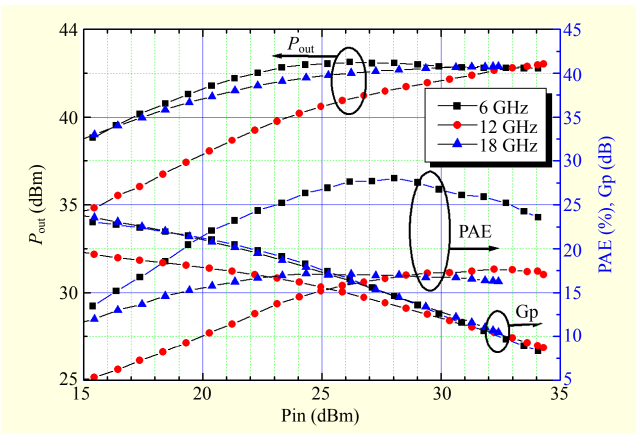

Fig. 12. Measured output power and PAE of the wideband HPA vs. the input power under the conditions of a pulse width of 100 µs and a duty cycle of 10%, and biased at *VD* = 30 V. Input power was swept from 15 to 34 dBm at 6 GHz, 12 GHz, and 18 GHz.

of the test fixture. For the CW measurements, the wideband MMIC HPA was attached to a copper-tungsten (CuW) carrier employing eutectic solder, and the carrier was assembled in an aluminum fixture with end-launched 2.9-mm k-connectors. An end-launched connector has an advantage in avoiding the cavity resonance that occurs by the inner wall of the text fixture. The text fixture is mounted on a heat sink plane made of aluminum with a fan for effective thermal dissipation. The CW-measured output power was significantly degraded compared to the pulse-mode measurement.

A second attempt at the test fixture used a different material and shape with a larger size. Copper/copper–molybdenum/copper (CPC) and copper (Cu) were used for the carrier and

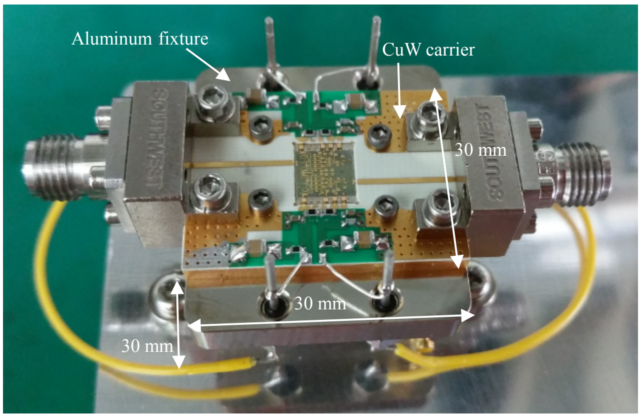

Fig. 13. Photograph of the test fixture assembled CuW carrier pasted on Ni-plated aluminum fixture, which is mounted on an aluminum heat sink. Fixture size is around 30 mm × 30 mm × 30 mm.

test fixture, respectively.

The thermal conductivities of the carriers were 197 W/mk and 220 W/mK for CuW-10 (10% Cu and 90% W) and CPC (Cu/CuMo/Cu, 1:4:1), respectively [12]. The thermal conductivity of Cu is known to be around twice that of aluminum. The Cu test fixture was Ni-plated for anti-oxide and designed to have a bigger size than the aluminum fixture, whereas the CPC carrier had the same shape as the old version of the CuW carrier. The thickness of both carrier types is 2 mm.

Figure 13 shows a photograph of the CuW carrier assembled in the Ni-plated aluminum fixture with a small size of 30 mm × 30 mm × 30 mm. However, based on the authors' development experience regarding several types of narrow frequency band HPAs based on GaN technology, the small size of the test fixture was sufficient to precisely measure the power performances of the HPAs. Figure 14 shows the new version of the test fixture made from the CPC carrier and Cu fixture. The size of the fixture was 100 mm × 100 mm × 30 mm excluding the block with an 8-mm height for the connection of the RF connectors and DC feedthrough. A height of 30 mm was obtained through a thermal analysis assuming that the thermal heat spreads at an angle of 120 degrees to the bottom with a size of 100 mm × 100 mm. The fixture is mounted on a heat sink made of aluminum with a fan, similar to the older version.

The CW-measured results of the output power and PAE versus frequency for the two types of test fixture are shown in Fig. 15. The drain voltage (VDS) and gate voltage (VGS) were set to 30 and –2.6 V, respectively, and the input power was fixed to 30 dBm. The output power for the test fixture with the CPC carrier and Cu fixture was measured within a range of 40.4 dBm (11-W) to 43 dBm (20-W) at the operating frequency band of 6 GHz to 18 GHz, and the average output power was around 15 W. The PAE varies between 10% and 23% for the new fixture. The value of the output power

http://dx.doi.org/10.4218/etrij.16.2615.0020

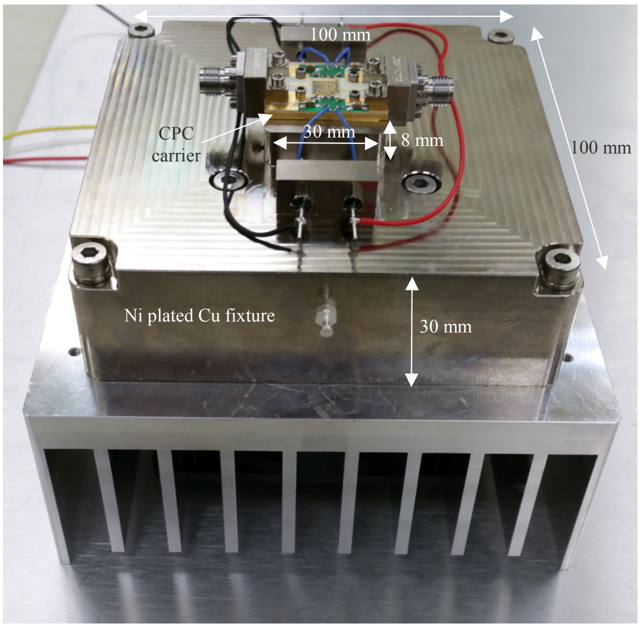

Fig. 14. Photograph of the test fixture assembled CPC carrier pasted on Ni-plated Cu fixture, which is mounted on a aluminum heat sink. Fixture size is around 100 mm × 100 mm × 100 mm.

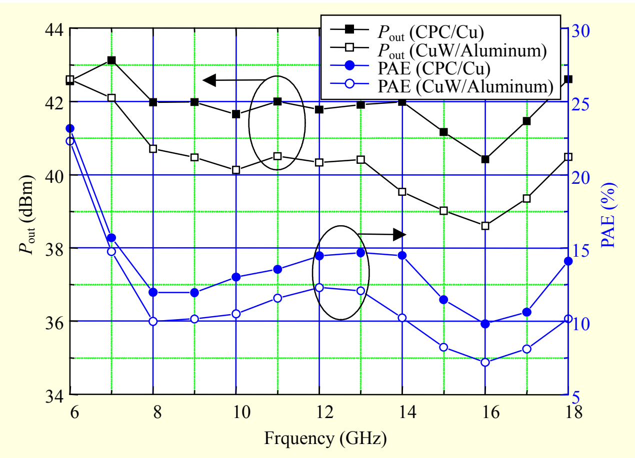

Fig. 15. Measured output power and PAE of the wideband HPA for two types of test fixtures with 30-dBm input power vs. frequency (CPC/Cu and CuW/aluminum are test fixtures with a CPC carrier mounted on a Cu fixture, and a CuW carrier on an aluminum fixture, respectively).

measured under CW conditions is similar to the pulse mode measurement in Fig. 9, whereas the efficiency has a slight difference.

A comparison between the CuW/aluminum fixture and the CPC/Cu fixture shows that the differences in the output power and PAE are around 2 dB and 4%, respectively, over the frequency range with the exception of 6 GHz to 7 GHz. At this low frequency, the power efficiency is relatively high, which indicates that a CuW/aluminum fixture with a small size has sufficient thermal capability for an HPA with a narrow frequency band and high power efficiency, even if it is not suitable for this wideband HPA.

IV. Conclusion

In this paper, we presented an ultra-wide MMIC high-power amplifier designed based on commercial 0.25-µm GaN technology with an average output power of 15 W. The amplifier demonstrates a saturation output power ranging from 11 W to 20 W, with a power-added efficiency of 10% to 23% under CW conditions over a frequency range of 6 GHz to 18 GHz. For the CW measurements, a CPC carrier and a Cu test fixture were designed considering the thermal problems, which provides similar power capability as a pulse mode measurement. To improve the input and output return losses, a balanced-type configuration with Lange couplers was adapted, and the HPA demonstrated good input and output return losses of lower than –15 dB. We believe this HPA chip with a wide operating frequency band and high-power performance will be a good candidate for realizing a transmitter module used in phased array jammer systems.

References

[1] N. Escalera et al., "Ka-Band, 30 Watt Solid State Power Amplifier," *IEEE MTT-S Int. Microw. Symp. Dig.*, Bosyon, MA, USA, June 11–16, 2000, pp. 561–563.

[2] C. Costrini et al., "50 W X-Band GaN MMIC HPA: Effective Power Capability and Transient Thermal Analysis," *Eur. Microw. Conf.*, Paris, France, Sept. 2010, pp. 408–411.

[3] K. Nakatani and T. Ishizaki, "A 2.4 GHz-Band 100 W GaN-HEMT High-Efficiency Power Amplifier for Microwave Heating," *J. Electromagn. Eng. Sci.*, vol. 15, no. 2, Apr. 2015, pp. 82–88.

[4] E. Reese et al., "Wideband Power Amplifier MMICs Utilizing GaN on SiC," *IEEE MTT-S Int. Microw. Symp. Dig.*, Anaheim, CA, USA, May 23–28, 2012, pp. 1230–1233.

[5] Hittite HMC7149 Data Sheet, Accessed Nov. 11, 2014. http://www.analog.com/media/en/technical-documentation/data-sheets/HMC7149.pdf

[6] S. Masuda et al., "Over 10 W C-Ku Band GaN MMIC Non-uniform Distributed Power Amplifier with Broadband Couplers," *IEEE MTT-S Int. Microw. Symp. Dig.*, Anaheim, CA, USA, May 23–28, 2010, pp. 1388–1391.

[7] G. Mouginot et al., "Three Stage 6–18 GHz High Gain and High Power Amplifier Based on GaN Technology," *IEEE MTT-S Int. Microw. Symp. Dig.*, Anaheim, CA, USA, May 23–28, 2010, pp. 1392–1395.

[8] U. Schmid et al., "Ultra-wideband GaN MMIC Chip Set and

High Power Amplifier Module for Multi-function Defense AESA Applications," *IEEE Trans. Microw. Theory Techn.*, vol. 61, no. 8, Aug. 2013, pp. 3043–3051.
[9] UMS, GH25-10 User Guide for the DK 3.1, ver. 3.1, Jan. 2014.
[10] J. Jeong et al., "A Compact C-Band 50 W AlGaN/GaN High-Power MMIC Amplifier for Radar Applications," *ETRI J.*, vol. 36, no. 3, June 2014, pp. 498–501.
[11] H.M. Le et al., "An X-Band High-Efficiency MMIC Power Amplifier with 20-dB Return Losses," *IEEE J. Solid-State Circuits*, vol. 26, no. 10, Oct. 1991, pp. 1383–1389.
[12] R.S. Pengelly et al., "A Review of GaN on SiC High Electron-Mobility Power Transistors and MMICs," *IEEE Trans. Microw. Theory Techn.*, vol. 60, no. 6, June 2012, pp. 1764–1783.

Jin-Cheol Jeong received his BS degree in electronics engineering from Youngnam University, Gyengsan, Rep. of Korea, his MS degree in information and communications from Gwangju Institute of Science and Technology, Rep. of Korea, and his PhD in radio science and engineering from Chungnam National University, Daejeon, Rep. of Korea in 1995, 1997, and 2009, respectively. He is currently a principal researcher with the Electronics and Telecommunications Research Institute (ETRI), Daejeon, Rep. of Korea. His research interests include the design and analysis of receiver and transmitter modules as well as MMIC components, such as multi-function chips and power amplifiers.

Dong-Pil Jang received his BS and MS degrees and his PhD in electronics engineering from Chungnam National University, Daejeon, Rep. of Korea in 1992, 1994, and 2007, respectively. He is currently a principal researcher with ETRI. His research interests include the design and analysis of satellite communication transponder systems and active array radar systems, as well as active components, such as MMIC power amplifiers, low noise amplifiers, solid-state power amplifiers, and transmit/receive modules operating up to the millimeter-wave range.

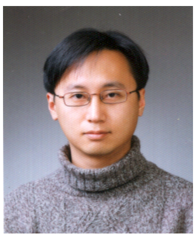

Dong-Hwan Shin received his BS and MS degrees in electronics engineering from Chungnam National University in 1996 and 1999, respectively. He is currently a principal researcher with ETRI. His research interests include the design and analysis of satellite communication transponder systems as well as active components, such as oscillators, MMIC power amplifiers, phase shifters, and attenuators operating up to the millimeter-wave range.

In-Bok Yom received his BS degree from Hanyang University, Seoul, Rep. of Korea in 1990, and his MS degreesand PhD from Chungnam National University in 2004 and 2007, respectively. Since 1990, he has been a principal research member and the head of the Satellite & Wireless RF Technology Research Section of ETRI. His research interests include microwave component design and satellite payload systems engineering.

Jae-Duk Kim received his BS and MS degrees in wireless communication engineering from Kwangwoon University, Seoul, Rep. of Korea in 2010 and 2012, respectively. He is currently a research engineer with the LIGNeX1 EW (Electronic Warfare) R&D Lab, Rongin, Rep. of Korea. His research interests include microwave applications such as power amplifiers and broadband systems.

Wang-Yong Lee received his BS degree in electronics engineering from Kyungil University, Kyungsan, Rep. of Korea, and his MS degree in information and electronic engineering from Ajou University, Suwon, Rep. of Korea in 1995 and 2007, respectively. He is currently a project leader with the LIGNex1 EW (Electronic Warfare) R&D Lab. His research interests include EW systems such as elecctronic attacks and electronic warfare support systems.

Chang-Hoon Lee received his BS degree in electrical engineering from Yonsei University, Seoul, Rep. of Korea, his MS degree in electronic engineering from Korea Advanced Institute of Science and Technology (KAIST), Daejeon, Rep. of Korea, and his PhD in electronic engineering from KAIST in 1999, 2001, and 2006, respectively. He is currently a team leader with the 2nd team in the 2nd R&D Institute of the Agency for Defense Development (ADD). His research interests include signal processing for electronic warfare and electronic warfare systems development.

http://dx.doi.org/10.4218/etrij.16.2615.0020